

# Picosecond charge variation of quantum dots under pulsed excitation

T. Kazimierczuk<sup>1,\*</sup>, M. Goryca<sup>1,2</sup>, M. Koperski<sup>1</sup>, A. Golnik<sup>1</sup>, J. A. Gaj<sup>1</sup>, M. Nawrocki<sup>1</sup>, P. Wojnar<sup>3</sup>, and P. Kossacki<sup>1,2</sup>

<sup>1</sup> *Institute of Experimental Physics, University of Warsaw, Hoża 69, PL-00-681 Warszawa, Poland.*

<sup>2</sup> *Grenoble High Magnetic Field Laboratory, B.P.166, 38-042 Grenoble, France.*

<sup>3</sup> *Institute of Physics, Polish Academy of Sciences, Al. Lotników 32/64, 02-688 Warsaw, Poland*

(Dated: January 18, 2021)

We present a spectroscopic study of excitation dynamics in self assembled CdTe/ZnTe quantum dots. Insight into details of kinetics is obtained from the time resolved micro-photoluminescence, single photon correlation and subpicosecond excitation correlation measurements done on single quantum dots. It is shown that the pulsed excitation in energy above the energy gap of the barrier material results in separate capture of electrons and holes. The capture of carriers of different charge take place at different delay from excitation.

PACS numbers: 78.55.Et, 78.67.Hc

## I. INTRODUCTION

Quantum dots (QDs) belong to the most intensely studied topics in the solid state physics. They owe their popularity to new physics involved and to a wide range of their possible applications in such fields as fabrication of efficient light sources, single photon emitters, information storage and processing<sup>1,2</sup>. A particular interest is related to the emerging field of quantum information<sup>3,4</sup>.

Self-assembled semiconductor quantum dots receive an important share of the research effort, due to efficient fabrication methods by modern epitaxial growth techniques and possibilities of integration with existing electronics. QD studies started from the prototypical InAs/GaAs material system, and were quickly extended over the entire families of III-V and II-VI semiconductors<sup>5,6</sup>. Among the physical phenomena studied in the quantum dot research, those related to light emission represent an important part, both under resonant and non-resonant excitation.

All-spectroscopic methods are well suited to study excitation and light emission processes in the QDs, in particular their dynamics<sup>7,8</sup>. The most precise information on the physical mechanisms involved in the excitation and light emission processes is usually supplied by single QD spectroscopy.

Basic QD spectroscopy methods include photoluminescence (both cw and time-resolved) under varied experimental conditions: excitation power, temperature, etc. In time-resolved studies the temporal resolution is usually determined by the type of detectors used (down to tens of ps for avalanche photo-diodes, to several picoseconds for streak cameras).

In some cases, more sophisticated spectroscopic techniques are necessary. For example, photon correlation measurements have been used to establish that in the case of non-resonant excitation of QDs, carriers are trapped separately rather than as whole excitons<sup>9</sup> (separate carrier capture in QDs was also demonstrated indirectly in cw experiments<sup>10,11</sup>). Standard form of pump-probe techniques is not much used, as absorption measurements of QDs present serious experimental difficulties<sup>12,13</sup>.

A technique more feasible for QD studies, similar to but not identical with pump-probe methods, is excitation correlation spectroscopy (ECS)<sup>14,15,16,17,18,19</sup>. In ECS, photoluminescence is excited by pairs of laser pulses separated by a controlled delay. It has been shown to be a powerful tool to investigate transient processes in semiconductors, especially excitonic recombination<sup>16,20</sup>. It has advantage of outstanding temporal resolution limited only by the properties of light pulses. However, not all the possibilities offered by ECS have been exploited so far. For instance, the order of carrier trapping in the excitation processes has not been studied to the best of our knowledge.

In this work, we profit from the excellent temporal resolution of the excitation correlation spectroscopy and apply it to a study of population dynamics in single CdTe/ZnTe quantum dots (QDs). In particular we study dynamics of carrier trapping by a QD under non-resonant pulsed excitation. The choice of the CdTe/ZnTe system is motivated by its two advantages with respect to the classical InAs/GaAs one. First, light emission in the visible range (red to green), and second, more robust excitonic states assuring efficient light emission at higher temperatures.

## II. SAMPLES AND EXPERIMENTAL SETUP

The studied sample contained an MBE-grown single layer of self-assembled CdTe/ZnTe QDs. The sample growth was described in detail in Ref. 21. The density of quantum dots was estimated to be about  $5 \times 10^9 \text{ cm}^{-2}$ . Measurements were performed on a sample immersed in superfluid helium (at 1.8K). A reflection microscope, immersed together with the sample, assured a spatial resolution better than  $0.5 \mu\text{m}$ . A frequency-doubled Sapphire:Ti femtosecond laser was used for pulsed above-barrier excitation. In excitation correlation experiments, the sample was excited by pairs of pulses with a controlled temporal separation (delay) between the pulses in a pair. Consecutive pairs were separated by the laser repetition period 13.6 ns. Time-integrated photolumines-

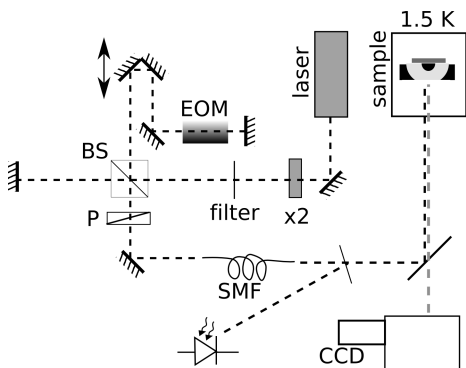


FIG. 1: Experimental setup used in excitation correlation experiments. The electro-optic modulator (EOM) was used to stabilize beam intensity probed after passing by a single mode fiber (SMF). BS denotes 50/50 beam splitter and P linear polarizer.

cence (PL) spectra were then recorded by a CCD camera as a function of the delay. The experimental setup is presented on Fig. 1.

Laser pulses were split in pairs in a Michelson interferometer setup. The length of one arm of the interferometer was varied by moving a corner-cube retroreflector mounted on a motorized translation stage. The setup allowed us to achieve a controlled delay up to 4 ns. Beams from two arms of the interferometer were combined again on a 50/50 beamsplitter forming a train of pairs of pulses. The joint beam was then transmitted through 50 cm of single-mode optical fiber acting as a spatial filter to assure a precise overlap of two laser spots on the sample. The width of each laser pulse at this point was estimated as 0.5 ps. The most challenging task in such experiment was to assure the stability of the excitation of a single quantum dot. Due to imperfections in optical alignment, the variation of the delay between the pulses led to changes in the efficiency of coupling to the fiber. This effect was canceled by introducing an electro-optical modulator into the variable-length arm of the interferometer, to stabilize the intensity of the laser after the fiber. As a result, a good stability of excitation of a single quantum dot was maintained over the measurement time which could exceed 6 hours.

In case of the single photon correlation measurements, a Hanbury-Brown&Twiss detection scheme<sup>22</sup> was used. The photoluminescence from the sample was split on a 50/50 beamsplitter and resolved by two monochromators equipped with avalanche photodiode (APD from Perkin Elmer or IdQuantique) single photon detectors. The APDs were connected to START/STOP inputs of TimeHarp 200 time counting system. An electrical delay introduced in the STOP signal allowed us to detect photons at negative delay values.

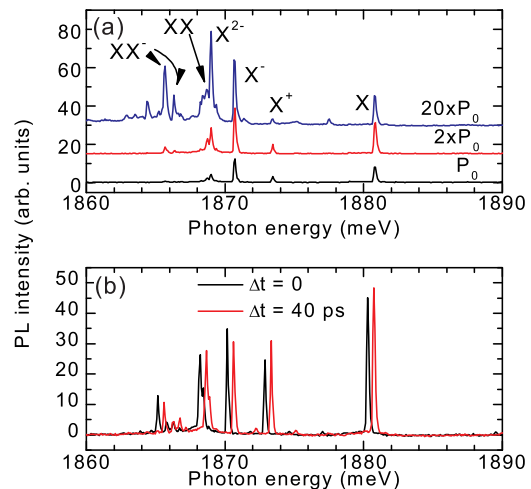


FIG. 2: (color online) (a) PL spectra of a single QD under different excitation intensities. (b) PL spectra excited by pair of laser pulses with temporal separation  $\Delta t$ . The  $\Delta t = 0$  ps spectrum was shifted horizontally for clarity by  $-0.5$  meV.

### III. PHOTOLUMINESCENCE SPECTRUM OF A SINGLE QD

Microphotoluminescence spectra of QD ensembles, limited by the size of the excitation and detection spots, revealed an inhomogeneously broadened distribution with a characteristic line structure. A low density of the lines in the low energy tail of the PL band allowed us to find well isolated sets of lines originating from single quantum dots. An example PL spectrum of a single quantum dot is presented on Figure 2. The lines were identified as originating from recombination of neutral and charged excitons and biexcitons, as marked in the figure. The identification was based on relative emission energies, in-plane anisotropy effects, and photon correlation measurements.

The lines emitted by the QD in the neutral or singly charged state were first tentatively identified on the basis of the characteristic pattern of their emission energies, observed in previous experiments on similar samples<sup>23</sup>, in particular with charge-tuning<sup>24</sup>. The identification of the lines related to neutral exciton (X) and biexciton (XX) transitions was confirmed by characteristic in-plane anisotropy effects. In case of a quantum dot of  $C_{2v}$  symmetry, both X and XX lines are split in linearly polarized doublets, originating from the fine structure splitting (FSS) of the excitonic state<sup>25</sup>. The experimental resolution did not allow us to observe the splitting directly. However, the components of the doublets could be observed in linear polarizations parallel and perpendicular

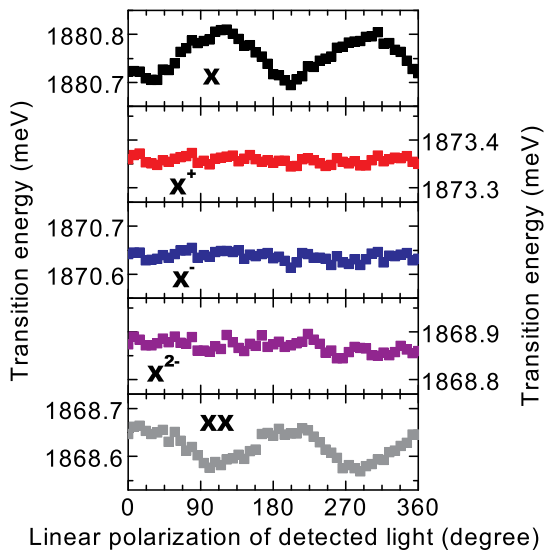


FIG. 3: (color online) Measured transition energy as a function of detected light polarization. Oscillatory behaviour indicates a small anisotropic splitting.

to the QD anisotropy axis. At intermediate polarization angles, each doublet was observed as a single broadened line at an intermediate spectral position. This effect leads to oscillations of the apparent X and XX transition energies as a function of orientation of detection polarization, as presented in Fig. 3. As expected, no energy oscillations were observed in case of charged excitons, in particular  $X^+$  and  $X^-$ , which contain pairs of identical carriers in singlet states. An argument supporting the assignment of trion signs is a negative optical orientation of  $X^-$  line, observed at quasi-resonant excitation through a neighbor dot<sup>23</sup>. The negative optical orientation had been observed for negative trions in many QD systems<sup>26</sup> and is related to electron-hole flip-flop process.

Some linear polarization effects were also observed for the doubly charged exciton  $X^{2-}$  line. However, they are beyond the scope of this work<sup>27</sup>.

Further data supporting the identification of the lines were obtained from photon correlation measurements. In our experiments, the quantum dot was excited by picosecond pulses of light and photoluminescence photons related to selected excitonic lines were counted by two detectors. Example results of such experiments are presented in Fig. 4, in the form of histograms of detection events of pairs of photons from the two transitions as a function of their temporal separation (number  $N$  of laser repetition periods). Due to pulsed excitation, time delay between the two emitted photons is close to integer multiples of the repetition period. A clear antibunching

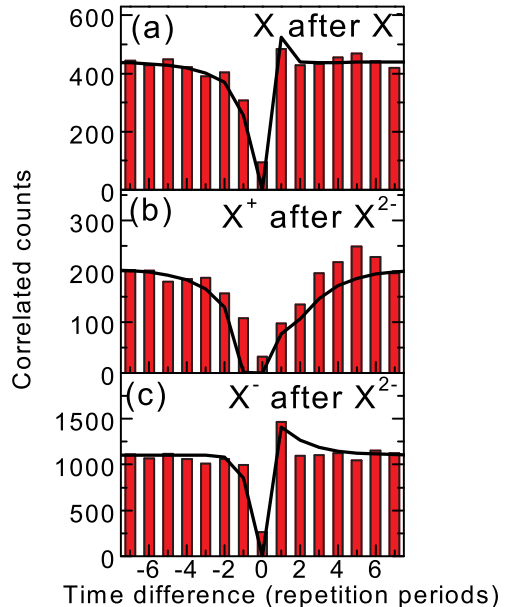


FIG. 4: (color online) Typical photon correlations related to change of charge state. Negative time distance denotes pairs with inverted photon order, e.g.  $X^-$  after X in case of (a). Solid lines were calculated within a model adapted from Ref. 9 with parameters  $\alpha = 0.80$ ,  $\beta = 0.86$ , and  $\xi = 0.26$ .

(suppression of the peak) at zero delay confirms unequivocally that we deal with a single photon emitter. Similar antibunching was observed for autocorrelation experiments, whereas cascade emission was witnessed by a characteristic bunching (enhancement of the central peak) in XX-X cross-correlation histograms (not shown). The  $X^{2-}$  line was identified using the cross-correlation histograms presented in Fig. 4. Besides the central antibunching, they show longer time-scale effects, extending over several repetition periods. Such effects are known to originate from QD charge variation<sup>9</sup>. The relatively high probability of the observation of correlated photons emitted after adjacent pulses in different charge states indicates an effective capture of single carriers. In particular, recombination of a neutral exciton after recombination of a negative trion requires only a single hole capture while a capture of three carriers is necessary if the emission order is opposite. Therefore corresponding probabilities of the events are respectively higher ( $N = +1$  peak at Fig. 4a) and lower ( $N = -1$  peak at Fig. 4a) than the probability in stationary state ( $N \rightarrow \infty$ ). The similarity of  $X^- - X^{2-}$  and  $X - X^-$  correlation histograms supports the assignment of the line  $X^{2-}$  to the doubly charged exciton. This assignment is confirmed by relatively long characteristic time-scales of the  $X^+ - X^{2-}$  correlation his-

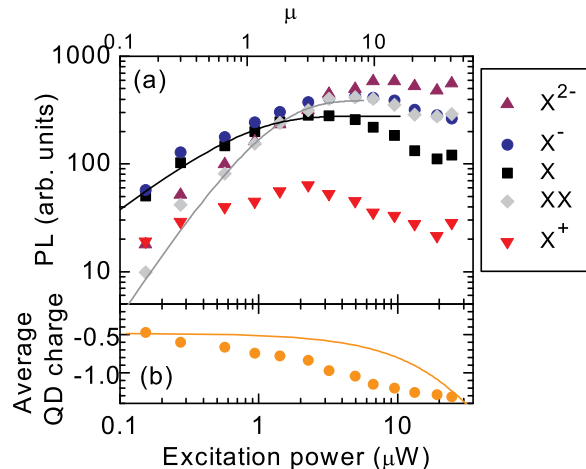


FIG. 5: (color online) (a) Photoluminescence intensity of various excitonic lines and (b) estimated average QD charge state versus excitation (pulsed laser) mean power. Solid line was calculated within a model described in Section V B and shifted vertically for clarity.

togram, as it is related to the largest change of the QD charge.

These qualitatively discussed correlation histograms can be simulated by a rate-equation model described in Ref. 9. We adapted this model by extending the possible states to incorporate transitions in  $+1$  and  $-2$  charge states. Free parameters of the model include probabilities of capturing an electron, a hole or a free exciton. Solid lines in Fig. 5 are calculated with probability values taken from Ref. 9. The results of the simulation confirm the predominant role of the single carrier trapping. They depend weakly on exact value of free exciton capture probability. A similar model is used in Section V C to simulate time profile of excitation correlation results.

The simplest experiment which gives an insight into the excitation dynamics is the measurement of photoluminescence spectra at various intensities of the pulsed excitation. A typical dependence of the intensity of selected excitonic lines on excitation power is presented in Fig. 5(a). In the lowest excitation limit, intensities of the PL lines exhibit power-like dependence. In case of  $X$ ,  $X^+$ , and  $X^-$  transitions, the dependence is linear. Two intensities ( $X^{2-}$  and  $XX$ ) increase super-linearly. The super-linear dependence observed for the  $X^{2-}$ -line is not surprising in view of a large number (four) of carriers necessary to form the  $X^{2-}$ -complex. Most of these results are in agreement with typical behavior expected for single exciton complexes and for biexcitons when the capture of whole excitons is significant<sup>9,28,29</sup>. A further increase of the excitation power leads to saturation of the line intensities. This behavior is related to the fact that each excitation

pulse results at most in one recombination cascade (the excitation time is much shorter than the recombination time). Therefore after one pump pulse only one photon related to a determined transition may be emitted. Nearly quadratic dependence of biexciton PL intensity indicates a need for including process of free exciton capture in addition to single carrier capture evidenced by photon correlation experiments. One should note that even a relatively small exciton capture rate may dominate over single carrier capture rates at low excitation power in multi-step excitation process, e.g. in case of  $XX$  formation.

At medium and high excitation power, the lines corresponding to negatively charged states of the QD become relatively more intense. This effect can be analysed quantitatively in terms of the average charge of emitting QD states calculated as:

$$\bar{q}_{QD} = \frac{0 \cdot I_X + 1 \cdot I_{X^+} - 1 \cdot I_{X^-} - 2 \cdot I_{X^{2-}}}{I_X + I_{X^+} + I_{X^-} + I_{X^{2-}}} \quad (1)$$

where  $I_S$  is PL intensity of line  $S$ . This formula approximates the averaged charge state of the quantum dot between excitation events since only the fundamental transition of each observed charge state is taken into account. No matter which was the highest state in a recombination cascade, its last step must be one of the final transitions:  $X$ ,  $X^+$ ,  $X^-$  or  $X^{2-}$ . Fig. 5 presents the average QD charge state as a function of excitation power. The effect of QD becoming negatively charged under strong excitation has been observed<sup>10</sup> but the underlying mechanism cannot be determined without more detailed studies. It may be caused by a modification of the electrostatic environment of the quantum dot (similarly to that known for quantum wells<sup>30,31</sup>). However, a mechanism inherent to the quantum dot itself is also possible. It is related to the apparent absence of doubly positively charged states of the quantum dot, while doubly charged negative trions have been identified. The difference between number of bound states in positively and negatively charged QD is predominantly caused by the small valence band offset in the CdTe/ZnTe system.

#### IV. MEASUREMENTS OF EXCITATION DYNAMICS

Excitation dynamics of the QDs was studied by means of excitation correlation experiments. As explained in Section II, a selected QD was excited by pairs of laser pulses. Time-integrated PL intensity was measured as a function of temporal separation  $\Delta t$  between the two pulses in the pair. Plots of such dependence over the full temporal range are presented in Fig. 6(a).

Features on two characteristic time-scales can be distinguished: a dip several hundreds of ps wide, and a much sharper feature, both centered at zero delay. The main effect is the relatively wide dip in the PL signal. Its width is comparable to the radiative lifetime of excitonic states

(Fig. 6(b)). The effect arises near the saturation regime when virtually each laser pulse excites the QD to a higher state. A qualitative explanation can be based on the fact that if the second pulse in a pair arrives prior to the excitonic recombination then the second pulse does not contribute to the intensity of the X transition. On the contrary, when pulses are separated by a few nanoseconds, they act independently and therefore the recorded PL intensity is doubled with respect to single pulse excitation. Thus, in the simplest approach the dip should be described by an exponential function which may be directly compared to the decay of the photoluminescence. This is shown on Figure 6(b-c) where the dashed line presents a profile obtained by fitting a monoexponential decay for  $|\Delta t| > 75$  ps of the X profile from Fig.6a.

The second time-scale in the experiment is in the range of tens of picoseconds. An additional variation of the PL intensity is observed within this scale, as presented in Fig. 7(a). The signal is increased or decreased depending on the excitonic complex with which the PL line is related. A clear increase of the photoluminescence at zero delay is seen for  $X^-$  and  $X^{2-}$ . A decrease is seen for neutral exciton and  $X^+$ . However, no significant effect is observed for a sum  $\Sigma_{PL}$  of intensities of photoluminescence lines related to all the observed charge states of the quantum dot (neutral and charged). This sum is shown on Figure 7 and its temporal variation is limited only to the slow component related to the excitonic decay. Invariability of the sum suggests that the effect is related to the QD charge state. Therefore we analyzed the averaged QD charge state versus pulse separation. The calculated charge state is shown in Fig. 7(b) and demonstrates a decrease of the averaged charge of the quantum dot when the pulses are in coincidence. The characteristic time of the feature appearing on the plots is the same as the lifetime of barrier luminescence, observed on similar samples<sup>32</sup>. Therefore we might associate this feature to the process of the carrier capture by the QD. The marked variation of the QD charge state during the pulse suggests a possibility of non-synchronous capture of carriers of different charge. In other words we wish to examine consequences of a delay between the arrival of holes and electrons in the QD.

We parameterized the short-timescale feature using the following procedure. In the first step we subtracted a baseline originating from long-timescale effect. We assumed for simplicity the same characteristic long-timescale profile for each emission line and rendered it by a total PL signal  $\Sigma_{PL}$ . We rescaled the total PL signal for each emission line by a constant factor to fit data points in a range  $100 \text{ ps} < |\Delta t| < 125 \text{ ps}$ . The rescaled temporal profile was then subtracted from the profile of the analyzed line. In the second step, we fitted an empirical function  $a \exp(-|\Delta t|/b)$  to the refined data, obtaining an amplitude  $a$  and a time constant  $b$  for each experimental scan. The results of this procedure are presented in Fig. 7(c-d) versus excitation power.

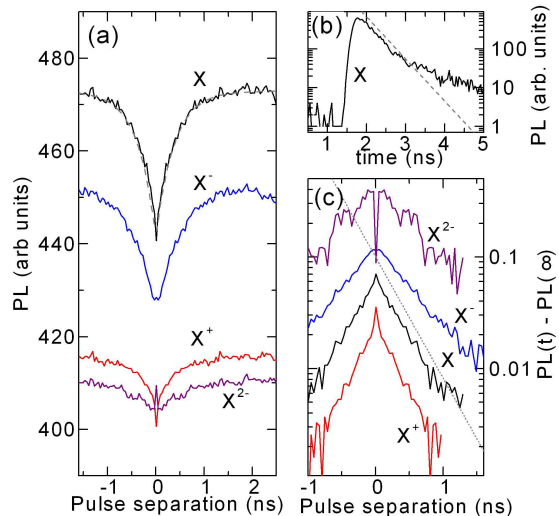


FIG. 6: (color online) (a) Excitation dynamics over long time-scale. Presented data was symmetrized (averaged values for  $t$  and  $-t$ ) for clarity. (b) Photoluminescence decay after a single laser pulse for neutral exciton recombination. (c) Effect of two pulse excitation in a semi-logarithmic scale. The dashed lines on all panels correspond to decay with 400 ps time constant.

## V. MODEL DESCRIPTION

Experimental intensity-vs-delay plots, presented in the previous Section, exhibit two main characteristic features, centered around zero delay: (i) a sub-nanosecond decrease, common for most of the PL lines (with a characteristic time comparable to the PL decay time), (ii) a feature on the scale of tens of picoseconds, related to the variation of the QD charge state. A complete model description of the observed features is complex and requires certain assumptions concerning excitation mechanisms of the quantum dot, its relaxation channels and their characteristic times. Therefore, to achieve a better insight in the physical mechanisms involved, we first discuss simplified versions of the model, describing selected characteristic features of the data. In part (A) we discuss sub-nanosecond effects in the model neglecting details of the excitation process. In part (B) we show how a delay between the capture of electrons and holes results in a fast variation of the averaged charge of the quantum dot. The amplitude of this variation is described in a simplified model, in which both carrier capture profiles are completely separated in time, and only their integrals are meaningful. In part (C) we include an analysis of the temporal profiles and discuss characteristic times of the carrier capture.

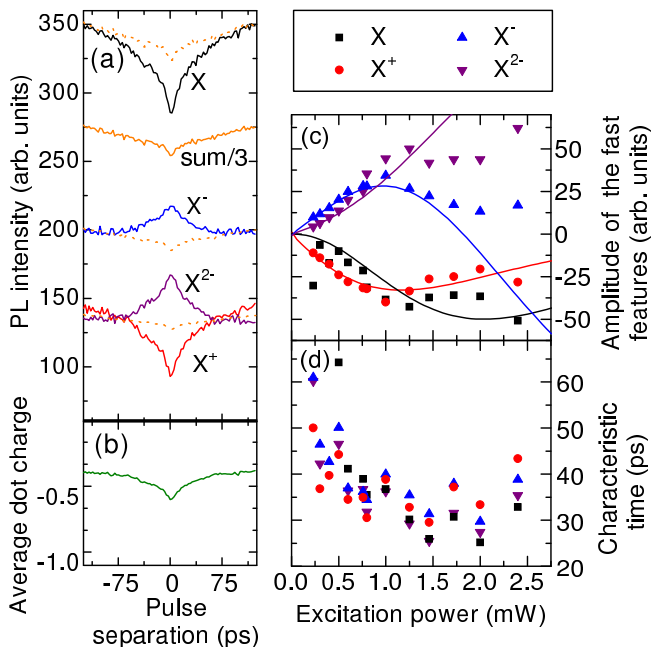


FIG. 7: (color online) Picosecond scale photoluminescence dynamics: (a) example result of excitation correlation experiment for different excitonic transitions and their sum (b) average charge state calculated according to eq. (1). Power dependence of (c) amplitude and (d) time-scale obtained by fitting  $a|\exp(-\Delta t/b)|$  to baseline-corrected data (see text). Lines are calculated within a model described in Section V.B, with suitable x and y scale adjustments.

### A. Sub-nanosecond scale dynamics

The shape of observed long-scale PL dependence can be explained by introducing a simple analytical model. Here we neglect the effects related to the QD charge state and consider the QD energy spectrum as an infinite ladder of states, starting from the lowest (ground) state for a given QD charge. Leaving out the charge degree of freedom in this model is justified by a similar decay dynamics of all the observed states (Fig. 6(b)). Within this simple model, we assume that the number of captured e-h pairs after a single laser pulse does not depend on current QD state and is described by a probability distribution  $R(k)$ . For example, in case of free exciton trapping the probability of capturing exactly  $k$  e-h pairs is given by a Poisson distribution<sup>28,29,33</sup>

$$\mathcal{P}(k, \mu) = \frac{\mu^k}{k!} e^{-\mu} \quad \text{and} \quad \mathcal{P}(0, 0) = 1 \quad (2)$$

where the average excitation  $\mu$  is identified with the excitation power. In case of separate capture of electrons and holes in a dot with limited number of charge states, the probability distribution is close to the square of the Poisson distribution. The particular shape of the distribution does not change dramatically the sub-nanosecond effects. After the pulse, the QD relaxes towards the ground state by radiative decay. We assume for simplicity that all

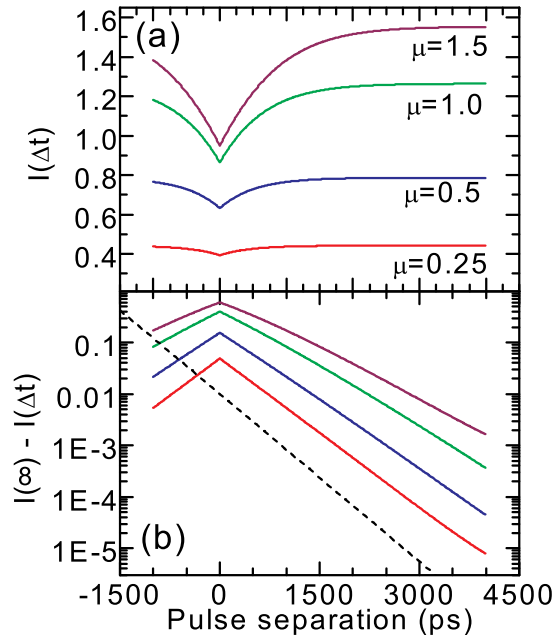


FIG. 8: (a) Simulated temporal profiles for different excitation intensities  $\mu$ . (b) The same simulated data in scale proper for a relaxation processes. Function  $\exp(-t/400\text{ps})$  is shown for reference (dashed line).

the excited states have the same lifetime of  $\tau = 400$  ps. Therefore the probability, that the quantum dot excited to  $n^{\text{th}}$  excited level emitted exactly  $l$  photons over time  $t$  is given by truncated Poisson distribution:

$$\tilde{\mathcal{P}}_n(l, t/\tau) = \begin{cases} \mathcal{P}(l, t/\tau) & \text{if } l < n \\ \sum_{i=n}^{\infty} \mathcal{P}(i, t/\tau) & \text{if } l = n \\ 0 & \text{if } l > n \end{cases} \quad (3)$$

Within this model, we derived the following expression for PL intensity of the first excited state (i.e. exciton state) in an excitation correlation experiment, when the two pulses are separated by  $\Delta t$ :

$$I(\Delta t) = (1 - R(0)) \left( 1 + \sum_{i=0}^{\infty} R(i) \tilde{\mathcal{P}}_i(i, \Delta t/\tau) \right) \quad (4)$$

Profiles of intensity versus  $\Delta t$ , simulated for different excitation intensities  $\mu$ , taking  $R(k) = \mathcal{P}(k, \mu)$ , are presented in Fig. 8.

It is interesting to note that the form of the simulated profiles is approximately mono-exponential (Fig. 8b). However, their slope decreases with increasing excitation intensity, and follows the lifetime of the system only in the limit of low excitation intensity. This finding should

be kept in mind when interpreting the measurements in which correlation excitation spectroscopy is used for determination of lifetimes<sup>16,20</sup>. The stability of our experimental setup was not sufficient to verify the predicted slope variation. On the other hand, the assumption of equal lifetimes of all contributing excited states is not fulfilled.

In spite of the simplicity of the approach, in which we neglect any possibility of the change of the charge state of the quantum dot, the above model reproduces quite well sub-nanosecond temporal profiles obtained in the excitation correlation experiment. It gives also a quite good prediction of the variation of the X and XX intensities versus excitation power up to the saturation level. The predictions of the model for X and XX lines are shown on Figure 5a by solid and dashed lines respectively. The introduction of the possibility of the change of the charge state of the quantum dot requires taking into account details of the carrier capture after the excitation pulse.

### B. Picosecond scale dynamics

The understanding of the short-scale PL dynamics requires a different approach. As mentioned previously, the effects on this scale are related to the QD excitation process (mainly the QD charge variation) rather than to the radiative relaxation after the first pulse.

Generally speaking, the excitation correlation signal results from a non-additive character (non-linearity) of the QD excitation by the two pulses. This non-linearity may be attributed to processes occurring in the barrier or in the QD. Here we assume that both pulses generate the same number of carriers in the vicinity of the QD, and the non-linearity originates in the QD itself. To describe the observed QD charge state variation, we assume that electrons and holes exhibit different trapping dynamics after a single excitation pulse. We will show that this approach allows us to explain in a simple way all the observed experimental features. In particular, we reproduce qualitatively the variation of the averaged charge of the quantum dot with excitation parameters: excitation power, delay between light pulses, and the ratio of energies of two consecutive light pulses.

The non-synchronous trapping of holes and electrons may be caused by different processes which result in different temporal profiles  $g_e(t)$  and  $g_h(t)$  of their capture rates. At this first stage, we will discuss a simple over-drawn case. We consider the carrier capture profiles as non-overlapping narrow pulses, with the electron trapping pulse delayed by time  $\tau_{e-h}$  with respect to the trapping of holes. The carrier trapping pulses can be described by standard rate equations

$$\begin{aligned} \dot{p}_+ &= -g_e p_+ + g_h p_0 \\ \dot{p}_0 &= g_e p_+ - (g_h + g_e) p_0 + g_h p_- \\ \dot{p}_- &= g_e p_0 - (g_h + \gamma g_e) p_- + g_h p_{2-} \\ \dot{p}_{2-} &= \gamma g_e p_- - g_h p_{2-} \end{aligned} \quad (5)$$

where we introduced an additional parameter  $\gamma$  to account for electron-electron blocking. The value of  $\gamma$  was set at 0.3 on the basis of relative intensities of neutral-to-charged exciton line. Under our assumptions, the rate equations can be integrated separately for the electron and hole capture pulses, producing matrices  $\mathbb{A}$  and  $\mathbb{B}$ , describing the influence of the pulses on the charge state probabilities.

$$\mathbb{A} = \exp \begin{bmatrix} 0 & \Gamma & 0 & 0 \\ 0 & -\Gamma & \Gamma & 0 \\ 0 & 0 & -\Gamma & \Gamma \\ 0 & 0 & 0 & -\Gamma \end{bmatrix}, \quad \mathbb{B} = \exp \begin{bmatrix} -\Gamma & 0 & 0 & 0 \\ \Gamma & -\Gamma & 0 & 0 \\ 0 & \Gamma & -\gamma\Gamma & 0 \\ 0 & 0 & \gamma\Gamma & 0 \end{bmatrix} \quad (6)$$

where  $\Gamma$  denotes the integral of capture rate over the pulse, assumed to be equal for electrons and holes and to be proportional to the intensity of the laser beam.

Each pair of laser pulses in the excitation correlation experiment will produce two pairs of carrier capture pulses. Depending on the separation between the two laser pulses, the hole trapping after the second pulse will take place before or after trapping of electrons from the first pulse. Thus, there are two possible orders of carrier trapping: hole-hole-electron-electron or hole-electron-hole-electron. The two cases can be described in terms of a recursive equation that binds charge state distributions before and after a pair of excitation pulses. For example, for the hole-electron-hole-electron ordering:

$$\begin{bmatrix} p_+^{(\text{after})} \\ p_0^{(\text{after})} \\ p_-^{(\text{after})} \\ p_{2-}^{(\text{after})} \end{bmatrix} = \mathbb{A} \cdot \mathbb{B} \cdot \mathbb{A} \cdot \mathbb{B} \cdot \begin{bmatrix} p_+^{(\text{before})} \\ p_0^{(\text{before})} \\ p_-^{(\text{before})} \\ p_{2-}^{(\text{before})} \end{bmatrix} \quad (7)$$

We computed stationary states in both cases and used the difference between them as a measure of the amplitude of the picosecond-scale feature. The results of the simulation are compared with the experimental results in Fig. 7(c), after an appropriate adjustment of both amplitude and power scales. A good agreement is achieved at low excitation power, while some discrepancies appear at higher power. They may originate from the absence of higher charge states in the model description. The model provides also a correct qualitative description of the observed evolution of the average QD charge state towards more negative values under increasing excitation power, as shown in Fig. 5(b). The enhancement of the negative QD states is obtained only if  $\tau_{e-h} > 0$ , that is if electrons are captured after holes.

An additional test of the model was provided by experiments in which the intensities of two consecutive light pulses were different. This eliminates the temporal symmetry of the obtained profiles. In our experiments, the power of one beam was kept constant and the power of the second one was set at different levels in a series of consecutive measurements. Typical experimental profiles, obtained for the power ratio 1:2, are shown on Fig.

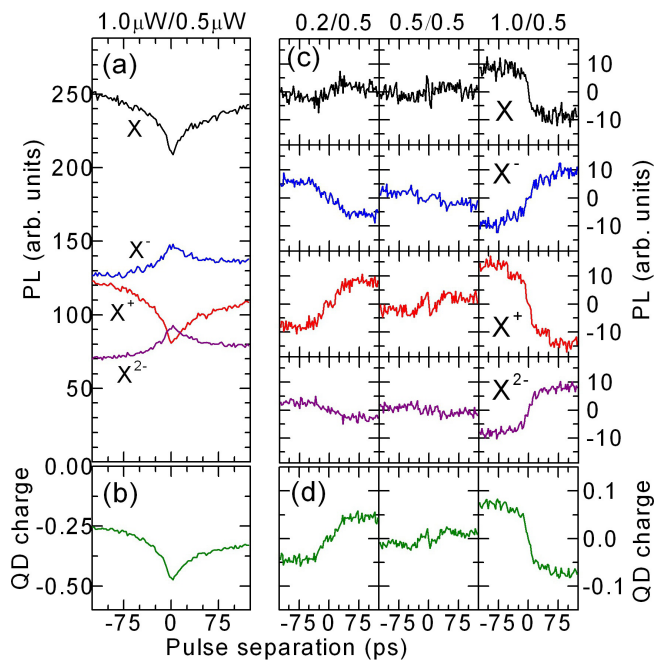


FIG. 9: (color online) (a,b) Results of excitation correlation experiment with two pulses of different intensities ( $0.5\mu\text{W}/1.0\mu\text{W}$  denotes pulse order for negative pulse separation). (c,d) Plots of effect asymmetry obtained by subtraction:  $PL(t) - PL(-t)$  for three sets of pulse intensities:  $0.2/0.5\mu\text{W}$ ,  $0.5/0.5\mu\text{W}$ , and  $1.0/0.5\mu\text{W}$ .

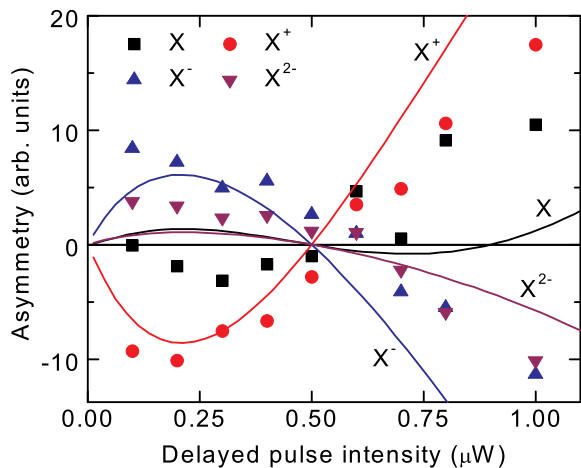


FIG. 10: (color online) Amplitude of asymmetry plotted against intensity of one of the pulses. Intensity of the other pulse was set to  $0.5\mu\text{W}$ . Solid lines are calculated within a model described in Section V.B and rescaled by a common factor.

9(a). The obtained profiles are clearly asymmetric. This asymmetry is better visible in the plots of difference between signals measured at opposite delays. An example is presented in Fig. 9(c) for different power ratio values. At ratio 1:1, as expected, the signal is almost zero for all the excitonic complexes. For ratio different than 1, the lines related to negative exciton complexes are stronger when the stronger pulse arrives second. At the same time, neutral and positively charged exciton lines are less intense. The signal asymmetry increases during the first tens of picoseconds, reaches a maximum for a delay of about 100ps and then decays with a decay time similar to the exciton recombination time. We extracted the asymmetry amplitude and compared it to the predictions of the model. The amplitude obtained for different exciton complexes and ratios of the light power in two beams is presented on Fig. 10 and marked by symbols. In the model, different powers of the two beams were simulated by taking different values of  $\Gamma$  (proportional to beam power) in two pairs of matrices  $\mathbb{A}$  and  $\mathbb{B}$  in equation 7. The results of the simulation are presented by lines on Figure 10. The agreement is quite good and supports our interpretation of separate capture of electrons and holes.

### C. Continuous rate equation model

The simple model discussed in section B was sufficient to analyze the amplitudes of the picosecond scale features observed in the excitation correlation experiment. However, to describe the temporal shape of the observed peaks, we need certain assumptions about the profiles of the carrier capture rates. Our data do not allow us to determine exact profiles, nevertheless they give some insight in the characteristic times. We propose here a rate equation model with simple exponential decays of the hole and electron capture rates  $g_h(t)$  and  $g_e(t)$ . They both start at the time of arrival of the light pulse and decay with different time constant  $\tau_h$  and  $\tau_e$  respectively. Such profiles could be related to the exponential decay of free carriers in the barrier material and/or wetting layer. The free carriers could be trapped by quantum dots or other centers. Direct measurements of the time resolved photoluminescence from the barriers in similar samples show a fast monoexponential decay<sup>32</sup>. Such decay would be a straightforward consequence of the above assumption if  $\tau_e \gg \tau_h$ , and then the measured PL decay was equal  $\tau_h$ .

In our continuous model, we consider 10 states of the quantum dot including ground and first excited states for the total QD charge  $+1$ ,  $0$ ,  $-1$ ,  $-2$ , and second excited states for the charge  $0$  and  $-1$ . This selection is based on the identification of the optical transitions observed in the spectrum. Following Ref. 9, we assume excitation by trapping of an electron, a hole or an entire exciton. Relative integrated rates of these processes are taken from Ref. 9. Due to the double pulse excitation, the temporal profile of excitation of each type is a sum of



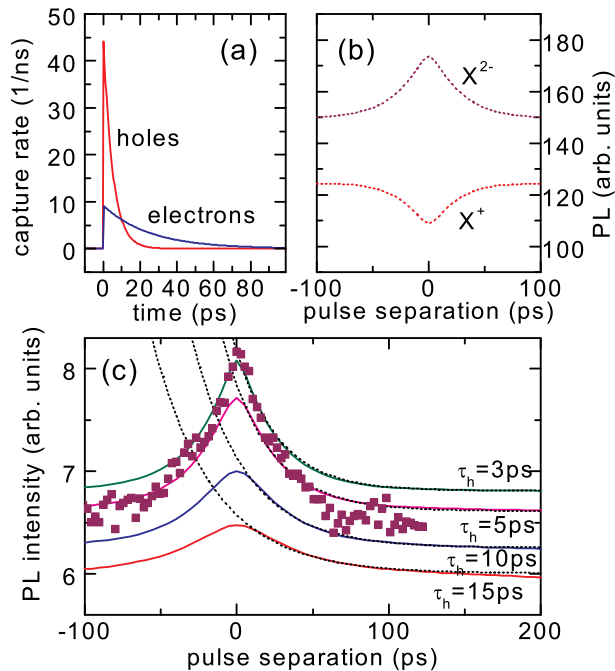


FIG. 11: (color online) Model of time dependence: (a) Capture rates for both carrier types after a single laser pulse. (b) Calculated photoluminescence of  $X^{2-}$  and  $X^+$  lines for various delays in two-pulse experiment. (c)  $X^{2-}$  simulations for  $\tau_e = 25$  ps and different parameters  $\tau_h$ . The curves are compared with experimental data (symbols) and simple exponential relaxation with time-scale  $\tau_e + \tau_h$ .

two exponential decays starting at arrival of subsequent laser pulses. The rate equations that include thus defined excitation and radiative recombination are integrated numerically. Photoluminescence intensities of various lines are found by integrating the respective radiative recombination over one repetition period, after finding a steady state of the system.

Example temporal profiles, calculated for the extreme charge states ( $X^+$  and  $X^{2-}$ ), are presented in Figure 11(b). A sharp increase of the intensity of  $X^{2-}$  is accompanied by a decrease of the  $X^+$  intensity. Both features have a similar shape which can be approximated by

an exponential function. The characteristic time of this function is determined by parameters  $\tau_h$  and  $\tau_e$ . However it is never smaller than the larger of them and it is close to the value of their sum :  $\tau_h + \tau_e$ . The amplitude of the peak decreases when values  $\tau_h$  and  $\tau_e$  become closer to each other. A comparison of the characteristic times obtained from simulations to the experimental ones allows us to conclude that the electron capture time (the longer one) is in the range of 20-40ps. The hole capture time is much smaller to assure a sufficient amplitude of the observed features.

## VI. SUMMARY

We performed a detailed time-resolved spectroscopic study of single CdTe/ZnTe quantum dots. The excitation dynamics was investigated by the time resolved micro-photoluminescence, single photon correlation and subpicosecond excitation correlation measurements. The time resolved experiments were done with excitation by ultrafast pulsed laser working at energy above the energy gap of the barrier material. The obtained temporal profiles of excitation correlation exhibit several characteristic features: sub-nanosecond decrease of the intensity common for most of the PL lines (with characteristic time comparable to PL decay time), and picosecond variation of the relative intensity of the lines related to excitons of different charge state. We propose a model describing observed features and demonstrate that it requires that the carriers are trapped separately. Moreover the capture of carriers of different charge take place at different delay from excitation. The detailed analysis of the temporal profiles let us conclude that the electron capture takes place in 20-40ps after excitation, while capture of hole is much faster.

## Acknowledgments

This work was partially supported by the Polish Ministry of Science and Higher Education as research grants in years 2006-2009 and by European Project No. MTKD-CT-2005-029671. One of us (PK) acknowledges the support from European Project No. FP7/2007-2013-221515 (MOCNA).

\* Electronic address: Tomasz.Kazimierczuk@fuw.edu.pl

<sup>1</sup> P. Michler, *Single Quantum Dots: Fundamentals, Applications and New Concepts*, vol. 90 of *Topics in Applied Physics* (Springer, New York, 2003).

<sup>2</sup> P. Michler, A. Kiraz, C. Becher, W. V. Schoenfeld, P. M. Petroff, L. Zhang, E. Hu, and A. Imamoglu, *Science* **290**, 2282 (2000).

<sup>3</sup> D. Loss and D. P. DiVincenzo, *Phys. Rev. A* **57**, 120 (1998).

<sup>4</sup> D. P. DiVincenzo, *Science* **270**, 255 (1995).

<sup>5</sup> P. M. Petroff, A. Lorke, and A. Imamoglu, *Phys. Today* **54**, 46 (2001).

<sup>6</sup> D. Bimberg, M. Grundmann, and N. N. Ledentsov, *Quantum Dot Heterostructures*, Quantum Dot Heterostructures

- (Wiley & Sons, New York, 1999).
- <sup>7</sup> P. Bajracharya, T. A. Nguyen, S. Mackowski, L. M. Smith, H. P. Wagner, U. W. Pohl, D. Bimberg, and M. Strassburg, *Phys. Rev. B* **75**, 35321 (2007).
  - <sup>8</sup> T.-E. Nee, Y.-F. Wu, C.-C. Cheng, and H.-T. Shen, *J. Appl. Phys.* **99**, 13506 (2006).
  - <sup>9</sup> J. Suffczyński, T. Kazimierczuk, M. Goryca, B. Piechal, A. Trajnerowicz, K. Kowalik, P. Kossacki, A. Golnik, K. Korona, M. Nawrocki, et al., *Phys. Rev. B* **74**, 085319 (2006).
  - <sup>10</sup> E. S. Moskalenko, L. A. Larsson, M. Larsson, P. O. Holtz, W. V. Schoenfeld, and P. M. Petroff, *Phys. Rev. B* **78**, 75306 (2008).
  - <sup>11</sup> G. Muñoz-Matutano, J. Gomis, B. Aln, J. Martinez-Pastor, L. Seravalli, P. Frigeri, and S. Franchi, *Physica E* **40**, 2100 (2008).
  - <sup>12</sup> J. Houel, S. Sauvage, P. Boucaud, A. Dazzi, R. Prazeres, F. Glotin, J.-M. Ortéga, A. Miard, and A. Lemaitre, *Phys. Rev. Lett.* **99**, 217404 (2007).
  - <sup>13</sup> B. Alén, F. Bickel, K. Karrai, R. J. Warburton, and P. M. Petroff, *Appl. Phys. Lett.* **83**, 2235 (2003).
  - <sup>14</sup> D. Rosen, A. G. Doukas, Y. Budansky, A. Katz, and R. R. Alfano, *Appl. Phys. Lett.* **39**, 935 (1981).
  - <sup>15</sup> A. Olsson, D. J. Erskine, Z. Y. Xu, A. Schremer, and C. L. Tang, *Appl. Phys. Lett.* **41**, 659 (1982).
  - <sup>16</sup> M. Jorgensen and J. Hvam, *Appl. Phys. Lett.* **43**, 460 (1983).
  - <sup>17</sup> S. Ideshita and Y. Masumoto, *J. Phys. Soc. Jpn.* **59**, 331 (1990).
  - <sup>18</sup> T. Mishina, H. Chida, and Y. Masumoto, *Phys. Rev. B* **48**, 1460 (1993).
  - <sup>19</sup> Y. Yamada, T. Mishina, Y. Masumoto, Y. Kawakami, J. Suda, S. Fujita, and S. Fujita, *Phys. Rev. B* **52**, R2289 (1995).
  - <sup>20</sup> H. Hirori, K. Matsuda, Y. Miyauchi, S. Maruyama, and Y. Kanemitsu, *Phys. Rev. Lett.* **97**, 257401 (2006).
  - <sup>21</sup> P. Wojnar, J. Suffczyński, K. Kowalik, A. Golnik, M. Aleszkiewicz, G. Karczewski, and J. Kossut, *Nanotechnology* **19**, 235403 (2008).
  - <sup>22</sup> R. Hanbury-Brown and R. Q. Twiss, *Nature* **178**, 1046 (1956).
  - <sup>23</sup> T. Kazimierczuk, J. Suffczyński, A. Golnik, J. A. Gaj, P. Kossacki, and P. Wojnar, *Phys. Rev. B* **79**, 153301 (2009).
  - <sup>24</sup> Y. Léger, L. Besombes, J. Fernández-Rossier, L. Maingault, and H. Mariette, *Phys. Rev. Lett.* **97**, 107401 (pages 4) (2006).
  - <sup>25</sup> D. Gammon, E. S. Snow, B. V. Shanabrook, D. S. Katzer, and D. Park, *Phys. Rev. Lett.* **76**, 3005 (1996).
  - <sup>26</sup> S. Laurent, O. Krebs, M. Senes, X. Marie, T. Amand, P. Voisin, and J.-M. Gerard, *Phys. Stat. Sol. (c)* **1**, 430 (2004).
  - <sup>27</sup> T. Kazimierczuk, A. Golnik, M. Goryca, J. A. Gaj, K. P., and P. Wojnar, *Acta Phys. Pol. A* **to be published** (2009).
  - <sup>28</sup> M. Grundmann and D. Bimberg, *Phys. Rev. B* **55**, 9740 (1997).
  - <sup>29</sup> M. Abbarchi, C. Mastrandrea, T. Kuroda, T. Mano, A. Vinattieri, K. Sakoda, and M. Gurioli, *J. Appl. Phys.* **106**, 53504 (2009).
  - <sup>30</sup> P. Kossacki, J. Cibert, D. Ferrand, Y. M. D'Aubigne, A. Arnoult, A. Waiela, S. Tatarenko, and J. A. Gaj, *Phys. Rev. B* **60**, 16018 (1999).
  - <sup>31</sup> W. Maślana, P. Kossacki, P. Plochocka, A. Golnik, J. A. Gaj, D. Ferrand, M. Bertolini, S. Tatarenko, and J. Cibert, *Appl. Phys. Lett.* **89**, 052104 (2006).
  - <sup>32</sup> K. Korona, P. Wojnar, J. A. Gaj, G. Karczewski, J. Kossut, and J. Kuhl, *Solid State Comm.* **133**, 369 (2005).
  - <sup>33</sup> C. Santori, G. S. Solomon, M. Pelton, and Y. Yamamoto, *Phys. Rev. B* **65**, 73310 (2002).